Pyrrolidinium Imides: A New Family of Molten Salts and Conductive Plastic Crystal Phases

D. R. MacFarlane,*,† P. Meakin,† J. Sun,† N. Amini,† and M. Forsyth‡

Department of Chemistry and Department of Materials Engineering, Monash University, Clayton, Victoria 3168, Australia

Received: October 23, 1998; In Final Form: February 2, 1999

A new family of molten salts is reported, based on the *N*-alkyl, *N*-alkyl pyrrolidinium cation and the bis(trifluoromethane sulfonyl)imide anion. Some of the members of the family are molten at room temperature, while the smaller and more symmetrical members have melting points around 100 °C. Of the room-temperature molten salt examples, the methyl butyl derivative exhibits the highest conductivity; at 2×10^{-3} S/cm this is the highest molten salt conductivity observed to date at room temperature among the ammonium salts. This highly conductive behavior is rationalized in terms of the role of cation planarity. The salts also exhibit multiple crystalline phase behavior below their melting points and exhibit significant conductivity in at least their higher temperature crystal phase. For example, the methyl propyl derivative (mp = 12 °C) shows ion conductivity of 1×10^{-6} S/cm at 0 °C in its higher temperature crystalline phase.

Introduction

Room temperature molten salts have been an area of interest both for fundamental reasons, associated with the factors that promote their low or nonexistent melting point and the intrinsic ion conductivity displayed by these ionic liquids, and also for application in a variety of electrochemical device fields. Molten salts, sometimes also referred to as ionic liquids, generally have long been of interest to Angell and co-workers because of their range of behaviors, in particular with respect to glass formation. Recently, Angell and co-workers[1−4] have investigated an interesting series of Li^+ molten salts for applications in lithium battery technology. In other recent work,[5−9] a family of room-temperature molten salts based on the imidazolium ring (**I**) have been developed with a view to applications such as photoelectrochemical solar cells and as media for "clean" industrial processes. These imidazolium systems hold something of a record for room-temperature conductivity ($\sim 8 \times 10^{-3}$ S/cm); however, some doubts remain about the chemical and electrochemical stability of the 1-alkyl, 3-alkyl imidazolium family because of possible reactions at the C(2) carbon. The 1-alkyl, 2-alkyl, 3-alkyl imidazolium salts solve this problem, but are of lower conductivity.

In recent contributions from our laboratories,[10−13] we have reported a large family of low-symmetry quaternary ammonium cation salts, many of which have subambient melting points; some members of the family are, in fact, glass forming. This work represented the first report of low molecular weight (carbon atom number < 12) ammonium cation salts being molten at room temperature. It was proposed that the depression of the melting point compared with various related compounds was due in part to disruption of the symmetry of the cation, this serving to interfer with crystal packing and thereby destabilize, relatively, the crystalline state. However, a second factor was clearly important in that work, the presence of the bis(trifluoromethane sulfonyl) imide ion (**III**) (otherwise often referred to as simply the "imide" ion). This was shown to be the origin of an at least 100 °C depression of the melting points in the ammonium salt family based on this anion, compared with the corresponding iodides. It was also, unexpectedly, the progenitor of much higher fluidity and conductivity than observed for related ions (for example the triflate ion) where various salts of the same cation were able to be prepared. The highest room-temperature conductivity observed in this family of compounds was 8×10^{-4} S/cm, more than 1 order of magnitude lower than closely related, in terms of molecular mass (slightly smaller), imidazolium salts. The difference between the ammonium and imidazolium cations, of course, is stark. The former cations have globular to rod-shaped geometries depending on the alkyl substituents involved, whereas the latter cations are almost planar for the lower molecular weight members, e.g., the methylethyl imidazolium case.

In the case of the imide ion, the origin of some of its interesting properties can be deduced in part from a recently reported crystal structure.[14] In this, it is clear that the charge delocalization expected in the imide ion extends only from the central nitrogen to the neighboring sulfur atoms and not to any great extent onto the four sulfonyl oxygen atoms. The result of this partial delocalization is that the charge is substantially buried within the molecule, shielded by the oxygens and terminal $-CF_3$ groups from Coulombic interactions with neighboring cations. This reduced interaction appears, therefore, to be associated with increased ion mobility and reduced lattice energy in the crystalline state.

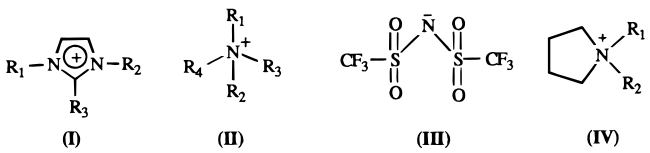

In this contribution, we report the preparation and characteriza-

* To whom correspondence should be addressed. E-mail: d.macfarlane@sci.monash.edu.au.

† Department of Chemistry.

‡ Department of Materials Engineering.

10.1021/jp984145s CCC: $18.00
Published on Web 03/26/1999

SCHEME 1

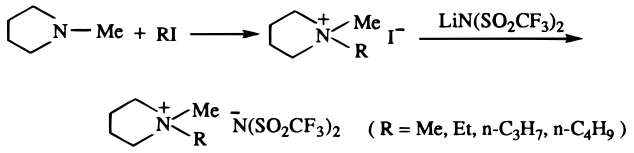

tion of another new family of molten salt-forming compounds, which conceptually bridge the structural gap between the fully three-dimensional ammonium ions and the close to planar two-dimensional imidazolium ions. The new family of salts is based on the pyrrolidinium cation (**IV**) where the two alkyl substituents range from methyl up to butyl. In some cases, these salts are shown to have melting points below room temperature. In some cases, they also show interesting conductive behavior in their crystalline state, in what we believe to be plastic crystal phases.

Experimental Section

Pyrrolidinium bis(trifluoromethane sulfonyl) imide salts were synthesized by reaction Scheme 1. The details of the synthesis and characterization of the compounds are presented in the appendix.

Conductance measurements were carried out in a number of locally designed multisample conductance cells, each designed to optimally cover a particular range of conductivities; in this work, conductivities between 10^{-9} and 10^{-1} S/cm were encountered. Each consists of a block of aluminum into which sample compartments were machined. The cell constant, b, of the embedded stainless steel blocking electrodes in each compartment was determined either by calibration before or after each sample measurement with 0.01 M KCl solution at 25 °C or by direct measurement of the empty cell capacitance, C_o. Cell constants were in the region of 1.0 cm^{-1} for the low sample impedance cell and 0.0025 cm^{-1} for the high sample impedance cell. Conductivities were obtained by measurement of the complex admittance of the cell between 20 Hz and 1 MHz using a HP4284A impedance meter. The temperature was either controlled at a set temperature or ramped at a steady 0.2 °C/min under the control of a Shimaden digital temperature controller. The type-T measurement thermocouple probe was located in the aluminum block close to the sample compartment. The conductance of the samples was determined from the first real axis touchdown point in the Cole−Cole plot of the impedance data. The complex electric modulus was calculated from the complex admittance, A^*, data via

$$M^* = i\omega C_o/A^* \qquad (1)$$

where M^* is the complex electric modulus, ω the angular frequency, C_o the empty cell capacitance ($=\epsilon_o/b$), and ϵ_o the permittivity of free space. Before the conductivity measurements, all samples were dried under vacuum for at least 3 days. No evidence of electronic conduction was found; in particular, the low-frequency behavior of the materials between the blocking electrodes was strongly capacitive as expected for an ion conductor/blocking electrode interface.

The densities of the liquid samples were determined by weighing a measured volume of the material. The Ostwald method was used in viscosity measurements of the liquid salts; glycerol (viscosity 954 mPa s at 25 °C), cyclohexanol (57.5 mPa s), 1,2-propylene glycol (40.4 mPa s), diethylene glycol (30.2 mPa s), ethanolamine (21.1 mPa s), ethylene glycol (16.1 mPa s), and glycerol−water solution (60 wt % glycerol, 8.82 mPa s) were used as standards.

A ML 400 MacLab/4e with Echem v1.3.1 Software was used for the electrochemical measurements. Glassy carbon was used as the working and counter electrodes, and the quasireference electrode was a silver wire (effectively forming a Ag/Ag^+ reference electrode in the melt). The scanning rate was 100 mV/s. Before each measurement, the samples were bubbled with dry, high-purity N_2 for more than 20 min to remove dissolved O_2.

A Perkin-Elmer differential scanning calorimeter (DSC) model 7 was used to measure the thermal properties at a scanning rate of 10.0 °C/min and using aluminum sample pans. Standard samples of oxalic acid dihydrate (mp 103 °C) and indium (mp 156.60 °C) were used for the calibration of temperature and power measurements in the DSC over the temperature range from 30 to 170 °C. A standard sample of cyclohexane (crystal−crystal transition temperature −87.06 °C and mp 6.54 °C) was used to calibrate the DSC over the temperature range from −150 to 40 °C. Before the DSC measurement, all samples were dried under vacuum at room temperature for at least 3 days.

Results and Discussion

We begin by characterizing and discussing the properties of these new substances as ionic liquids before proceeding to investigate their conductive behavior in the solid state.

Molten Salt Properties. The properties of the salts prepared in this work are summarized in Table 1. An acronym, P_{xx}, is used to distinguish between the salts by subscripting the number of carbons in each of the alkyl substituents. The dimethyl (P_{11}) and methyl ethyl derivatives (P_{12}) have relatively high melting points; however, with increasing alkyl chain length, the melting point has dropped below room temperature at the methyl propyl derivative. The melting points appear to fall steadily with increasing alkyl chain length, as observed previously in the ammonium salt family.[11] Typical DSC traces are shown in Figure 1. In the cases of P_{13} and P_{14}, it appears that the quenched molten salt is glass forming, the glass transition temperatures, T_g, measured on warming being −90 and −87 °C, respectively. The thermal analysis traces also show classic evidence of multiple crystallization and melting events in each case which we attribute to the existence of several polymorphs of the crystalline state in these compounds. Thus, in P_{13}, the exotherm at −67 °C is associated with the crystallization of the supercooled liquid to what is thought to be a metastable phase because of the subsequent further exotherm at −45 °C where it transforms to the low-temperature stable phase, denoted phase II. The progressive crystallization of first a metastable phase prior to appearance of the lowest energy, maximally ordered phase is well-known under these highly nonequilibrium conditions. Phase II then transforms into phase I at −18 °C, which subsequently melts at 12 °C. In the case of P_{12}, the quenched material shows a possible glass transition followed by sudden crystallization and transformation around −100 °C; however, as discussed further below, the glass transition is not that of the quenched liquid state. Since the sample is crystalline at room temperature at the beginning of the quench, the glass transition must result from quenched-in disorder of the high-temperature solid phase. P_{12} then shows a broad solid−solid transformation to phase I which is complete by 14 °C (entropy of transition 3.1 J K^{-1} mol^{-1}) and a final melting at 86 °C. The thermogram of P_{11} is much simpler than that of P_{12}, showing only a weak transition at 20 °C.

Conductivities of P_{13} and P_{14} in the liquid state are shown as a function of temperature in Figure 2, from which it can be seen that the conductivity is slightly higher for the P_{14} derivative.

TABLE 1: Properties of Pyrrolidinium Imide Salts[a]

acronym	structure	T_g (°C) (±2 °C)	phase II → phase I (°C) (±1 °C)	$\Delta S_{(II\rightarrow I)}$ (J K^{-1} mol^{-1})	phase 1 mp (°C) (±1 °C)	fluid density/ (g cm^{-3}) (20 °C) (±0.02)	viscosity (mPas) (±5%, 25 °C)	fluid conductivity (σ/10^{-4} S cm^{-1}) (±5%, 25 °C)	V_m (cm^3 mol^{-1}) (20 °C)	ΔS_f (J K^{-1} mol^{-1}) (±5%)
P_{11}	$(CH_3)_2C_4H_8\overset{+}{N}\overset{-}{N}(SO_2CF_3)_2$				132					40
P_{12}	$(CH_3)(C_2H_5)C_4H_8\overset{+}{N}\overset{-}{N}(SO_2CF_3)_2$	−102 (pc)	14	3.1	86					38
P_{13}	$(CH_3)(n\text{-}C_3H_7)C_4H_8\overset{+}{N}\overset{-}{N}(SO_2CF_3)_2$	−90	−18	4.0	12	1.45	63	14	280	43
P_{14}	$(CH_3)(n\text{-}C_4H_9)C_4H_8\overset{+}{N}\overset{-}{N}(SO_2CF_3)_2$	−87	−24	4.8	−18	1.41	85	22	300	41

[a] T_g = glass transition temperature; V_m = molar volume; $\Delta S_{(II\rightarrow I)}$ = entropy of phase II → phase I transition; ΔS_f = entropy of fusion.

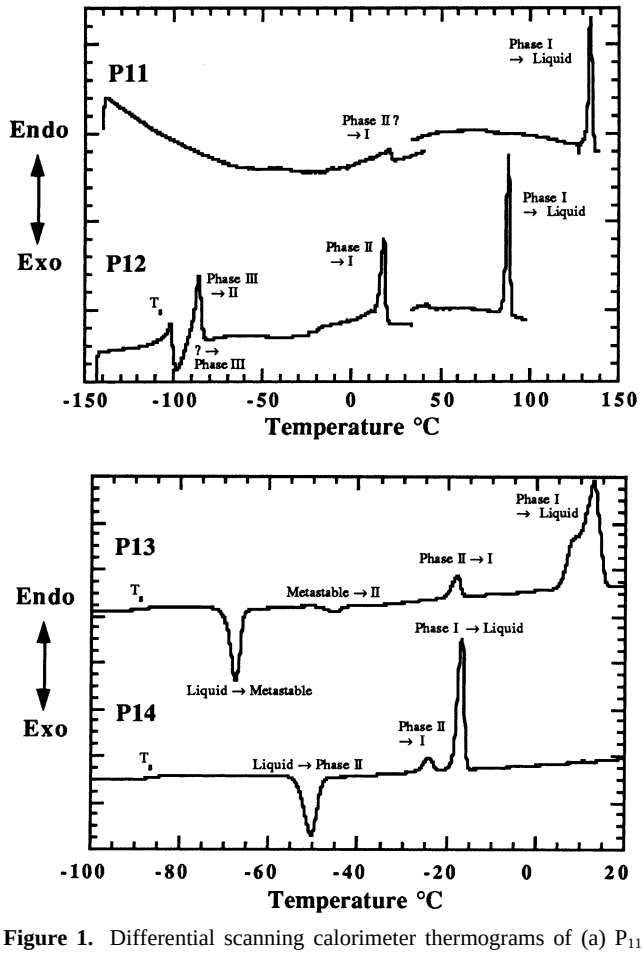

Figure 1. Differential scanning calorimeter thermograms of (a) P_{11} and P_{12} on warming at 10 °C after quenching from room temperature and (b) P_{13} and P_{14} on warming at 10 °C after quenching from the liquid state. Glass transition temperatures are obtained at the onset of the transition.

This is unexpected given its higher viscosity and glass transition temperature, evidence that the conductive and structural modes of motion are not completely coupled in these compounds. Elias and Elias have recently discussed[15] the extent to which Walden's rule, i.e., the constancy of the product $\Lambda\eta$ where Λ is the molar conductivity ($=\sigma V_m$), breaks down for the imidazolium chloride−$AlCl_3$ room-temperature molten salts. The deviations from constancy were attributed to the formation of complex species including ion pairs. Similar species are to be expected in the present systems.

At room-temperature, P_{14} has a conductivity of 2.2×10^{-3} S/cm. By comparison, the analogous imidazolium salt (methylbutyl imidazolium imide) has conductivity 3.9×10^{-3} S/cm (at 20 °C),[5] whereas an ammonium salt of comparable carbon number (butyldimethyl propylammonium imide, N_{1134}) has conductivity around 8×10^{-4} S/cm.[13] The smaller imidazolium cations, dimethyl imidazolium imide and methylethyl imidazolium imide, which are analogous to P_{11} and P_{12}, respectively, have still higher conductivities, around 8×10^{-3} S/cm at 20 °C. From this it would appear that the planarity of the imidazolium ring is vital in supporting the high conductivity exhibited by these compounds. The pyrrolidinium ring approaches this to an extent, but the presence of the substituents above and below the plane of the ring clearly restricts the mobility of this ring compared to its more planar imidazolium relative. The pyrrolidinium ring itself is not planar, with the nitrogen atom sitting above the plane of the four ring carbons; however, in the methyl pyrrolidinium series, structural models, Figure 3, show that the dihedral angle between the ring carbons, the nitrogen, and the methyl group is ca. 163°, indicating a close to planar arrangement of this subgroup.

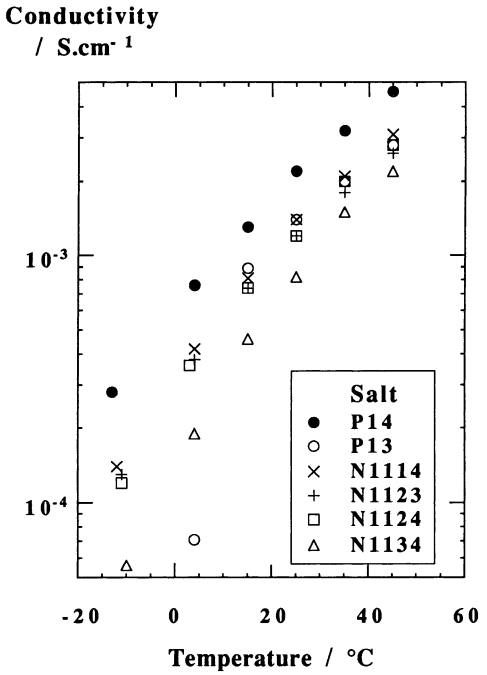

Figure 2. Conductivity versus temperature for methylpropyl pyrrolidinium imide (P_{13}) and methylbutyl pyrrolidinium imide (P_{14}) molten salts. The lowest temperature data point for P_{13} corresponds to a sample which has crystallized during the experiment (mp = 12 °C). Unpublished data for comparable ammonium salts is also shown.

Cyclic voltammograms are shown in Figure 4 for P_{14} cycled on a glassy carbon working electrode at 25 °C. Figure 3a shows that the P_{14} is electrochemically stable at least to −3.0 V and +2.5 V vs Ag/Ag$^+$. The electrochemical window of stability is

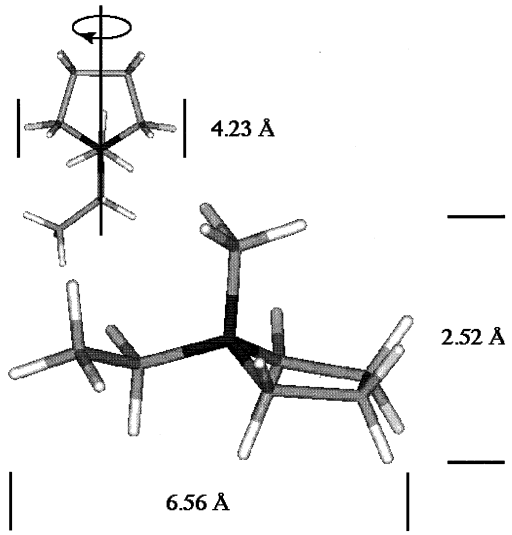

Figure 3. Representation of the methylpropyl pyrrolidinium cation. Structure was energy minimized within Discover 96 (Molecular Simulation Incorporated, San Diego).

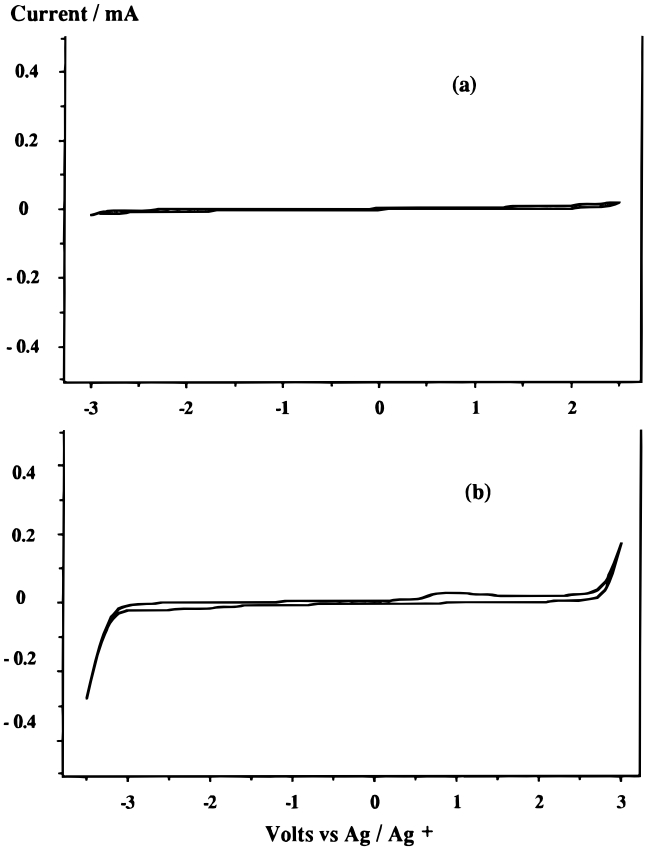

Figure 4. Cyclic voltammograms for P_{14} over various voltage ranges (a) cycling between and (b) extending the cycle to −3.5 V to +3.0 V vs Ag/Ag^+ at which point bulk oxidation and reduction processes in the −3 V and +2.5 V vs Ag/Ag^+ melt appear. The sign convertion used in this plot has positive currents = oxidation. Glassy carbon working and counter electrodes. Scan rate, 100 mV/s; $T = 25$ °C.

therefore in excess of 5.5 V. This window of electrochemical stability is one of the widest yet observed in a room-temperature molten salt. By comparison, the ammonium imide salts reported in ref 11 showed an approximately 4.5−5.0 V electrochemical window under similar experimental conditions. The pyrrolidinium salt is more stable by an additional 0.5 V toward reduction; this presumably reflects additional stability of the cation toward reduction. Extending the electrochemical excursion, Figure 4b, introduces (i) oxidation processes at ∼+2.75 V, followed by a corresponding reduction event around −2.0 V in the reverse scan and (ii) reduction processes in the melt just beyond −3.0 V, followed by a corresponding oxidation process around +1.0 V. The large potential differences between these melt breakdown processes and their corresponding reverse reactions indicate the strongly irreversible nature of the reactions involved.

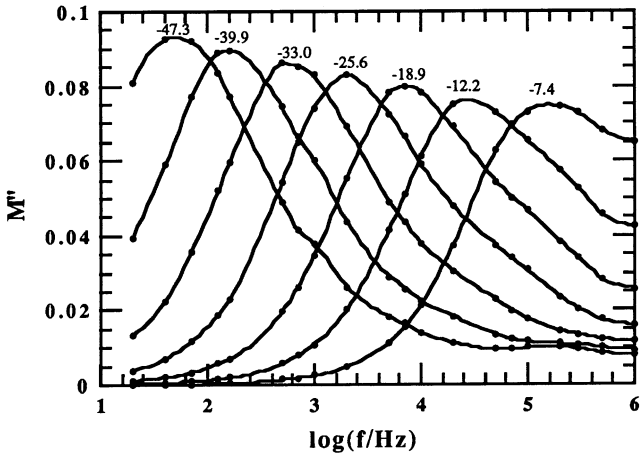

Figure 5. Imaginary part of the electric modulus versus frequency, plotted as isothermals, for methylpropyl pyrrolidinium imide.

Solid-State Behavior. As shown in Figure 2, there is an unexpectedly high conductivity evident in the P_{13} sample after it has crystallized during the experiment (the lowest temperature point). Exploring this further, samples were quenched from above their respective melting points in various cells designed to explore different conductivity regimes and admittance spectra gathered over a wide range of temperatures from below the glass transition temperature to above T_m. An example of the isothermal, variable frequency behavior of M″ is shown in Figure 5 for the solid forms of P_{13}. In accordance with the observed dc conductivity for the solid phases of these salts, the modulus spectra exhibit characteristic conductivity loss peaks. At the peak at each frequency and temperature, the following relationship holds:[16]

$$\omega_{peak} = \sigma_{dc}/\epsilon_o\epsilon_\infty \quad (2)$$

where ϵ_o and ϵ_∞ are the permittivities of free space and the material respectively and σ_{dc} is the limiting low-frequency conductivity. This relationship only holds exactly where the relaxation process is governed by a simple exponential. Figure 5 shows that the isothermal conductivity loss peak is somewhat broader than expected (1.14 decades of frequency) for a simple exponential (or Debye) process. This broadening is typical of many solid-state and viscous liquid ionic materials and is understood to be associated with an intrinsically nonexponential relaxation process for the motion of each ion and/or a distribution of relaxation times associated with different ionic sites and environments. Nonetheless, eq 2 holds approximately under these conditions.

From the admittance data set, the DC conductivity was obtained from the real axis touchdown in the impedance plane and is presented in Figure 6. From this figure, it is clear that the compounds all support a very substantial conductivity in the crystalline state just below their respective melting points. For example, P_{12} shows conductivity around 10^{-8} S/cm at room temperature, the conductivity rising steadily with activation

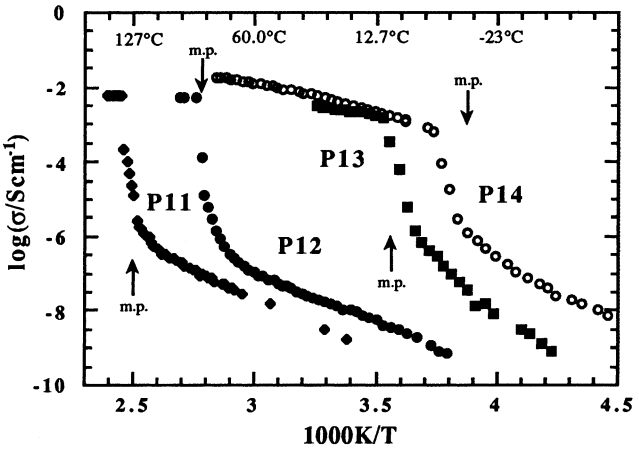

Figure 6. Log conductivity versus inverse temperature for pyrrolidinium imide salts in solid and liquid states. The DSC melting points are arrowed.

energy 47 kJ mol^{-1} up to about 10^{-7} S/cm at 70 °C. At this point, the conductivity begins to rise rapidly, reaching 7×10^{-3} S/cm at 88 °C; the DSC thermogram shows a sharp melting transition (onset 86 °C) in this region of temperature. There is no significant step in conductivity in the region of temperatures (14 °C) where the phase II → phase I transition is observed to take place thermally. P_{13} shows a similarly sharp step in conductivity around its final melting point from a solid-state conductivity which reaches 10^{-6} S/cm at 0 °C, just before melting begins. P_{14} shows almost identical behavior, the transition being shifted down in temperature by approximately 15 °C, consistent with the thermal analysis results. Interestingly, although all of the salts reach very similar conductivities just before the onset of melting, at any given temperature, for example, −20 °C, P_{14} is 1 order of magnitude more conductive in its crystal phase than is P_{13}, which is similarly more conductive than P_{12}.

Conduction in Plastic Crystals. Much of this phase transition and conductive behavior below the melting point is reminiscent of the observations of Ikeda and co-workers[17−21] in their investigations of plastic crystal behavior in ammonium compounds and also of Cooper and Angell[22] in their study of plastic crystal behavior in a methoxyethyl dimethyl ethylammonium compound. These groups have described the properties of a number of tetraalkylammonium and dialkylammonium compounds with anions such as the halides, Cl^-, Br^-, BF_4^-, I^-, and SCN^-. Via NMR relaxation measurements, Ikeda et al showed that plastic crystal phases (otherwise known as rotator phases or orientationally disordered phases) existed in these compounds over quite wide ranges of temperature up to the final melting point. The entropy of transition from the low-temperature ordered state into the partially disordered state (in some cases there existed a progression of several increasingly disordered states) was a substantial fraction of the final entropy of melting. The entropy of melting was, in most cases, in the vicinity of 2.5R (∼20 J K^{-1} mol^{-1}), characteristic of plastic crystals. The ionic conductivity of these compounds was found to be significant in their plastic crystal phase, for example, Et_2NH_2Br has $\sigma = 2.5 \times 10^{-7}$ S/cm at 400 K in its most disordered phase,[21] which extends from 342 to 481 K. The temperature dependence of conductivity was Arrhenius with activation energy = 58 kJ/mol. This activation energy was comparable to that observed from cation NMR $T_{1\rho}$ relaxation measurements. Trimethylethylammonium iodide exhibited two disordered phases both of which were ionically conductive.[19]

Plastic crystal phases have been known and described since the classic work of Timmermans.[23] They have characteristically very low entropies of melting (≤20 J K^{-1} mol^{-1}) and below the melting point often exhibit a series of solid−solid phase transitions. The highest temperature crystalline phase (often termed phase 1) is usually characterized by strong rotational disorder of the whole molecular unit or some substantial fragment thereof. Lying lower in energy than phase I are one or more states of higher order that become stable at lower temperature. The plastic crystal state is also understood to contain many lattice vacancies as a result of the rotational disorder, for which reason the material can exhibit plastic material properties, substantial self-diffusion coefficients, and, where appropriate, high ionic conductivity.

The behavior in the present pyrrolidinium family of compounds appears to bear many features in common with the observations of Ikeda and co-workers. All of the compounds investigated here exhibit at least one conductive crystalline phase and in several cases there is evidence of a series of conductive phases with increasing temperature. The entropies of melting of the present compounds, as listed in Table 1, are larger than the maximum of 20 J K^{-1} mol^{-1} normally expected for plastic crystals. The closest to this value is P_{12} with $\Delta S_f = 38$ J K^{-1} mol^{-1}. By comparison, the entropies of melting of a series of quaternary ammonium imide compounds reported by us in ref 13, which show only very low solid-state conductivity behavior ($\sigma < 5 \times 10^{-10}$ S/cm), are in excess of 50 J K^{-1} mol^{-1}; thus, it appears that the plastic crystal behavior in the present compounds is associated with the pyrrolidinium cation. However, it is likely that these compounds have additional configurational degrees of freedom associated with the imide ion which become active on melting. The compounds studied by Ikeda et al. contained either monatomic halide or other small anions, and the compounds typically otherwise showing plastic crystal behavior are usually relatively simple molecular crystals. Thus, in the case of the present pyrrolidinium compounds where the plastic crystal behavior is associated with only the cation and the anion itself is capable of contributing significantly to ΔS_f, it is likely that Timmerman's condition no longer represents a completely reliable indicator of plastic crystal behavior.

Angell and co-workers[24−28] have shown that the disorder present in a plastic crystal can be quenched into the structure by rapid cooling in much the same way that liquid-state disorder is quenched in a more normal glass-forming substance. The quenched plastic crystal can then exhibit a glass transition which is associated with the onset of the rotational motions responsible for the plastic crystal behavior. This would appear to be the phenomenon observed in the region of −100 °C in the thermogram of P_{12}, and for this reason the T_g noted in Table 1 has been indicated as pertaining to the plastic crystal phase.

Ikeda and co-workers were able to show via NMR measurements that the rotations responsible for the plastic crystal behavior involved the cation in the case of their ammonium salts. Therefore, we believe that the rotation involved in the rotationally disordered state in the present compounds is most likely to involve the cation executing a rotation about an axis which bisects the pyrrolidinium ring, as shown in the molecular representation in Figure 3. That there are several rotationally disordered phases suggests either a progression through a state of hindered rotation before full rotation is achieved in phase I and/or an involvement of other rotational modes of this molecule. Further details of these motions should be able to be illucidated via multinuclear NMR relaxation experiments. Ikeda and co-workers were able to definitively identify the charge

carrier responsible for the conduction in their plastic crystals as the cation in some cases (e.g., in $(CH_3)_4NSCN$[20]). However, in other cases (e.g., $(CH_3)_3NCH_2CH_3I$[19]) it appeared that it was the anion which was the only species able to undertake rapid translational motion in the two plastic crystal phases. It thus appears that either ion may be responsible for the conduction in the present materials; NMR self-diffusion measurements will be undertaken to shed further light on this issue.

We return now to the observation that when P_{13} and P_{14} are compared over a range of temperatures where both are in their conductive plastic crystal phase, it appears that the larger molecule P_{14} is the more conductive of the two by more than 1 order of magnitude. This indicates that the larger molecular cation in its rotationally disordered arrangement creates a greater degree of lattice expansion over the ordered phase and also thereby a larger number of lattice vacancies.

Conclusions

A new family of salts based on the pyrrolidinium family of cations and the bis(trifluoromethane sulfonyl) imide ion have been described. The methyl propyl (P_{13}) and methyl butyl (P_{14}) derivatives have subambient melting points and are thus stable molten salts at room temperature. P_{14} has the highest room temperature conductivity, and by analogy with trends seen in related families of compounds, it is possible that slightly higher conductivities may yet be observed somewhere in the vicinity of the P_{23} or P_{15} members of the family. All of the compounds described exhibit polymorphism in the crystalline state possibly including plastic crystal phases which are able to support substantial conductivity in its crystalline lattice via hopping between lattice vacancies. Given the large size and mass of the mobile ions involved, the conductivity exhibited by the plastic crystal material, of the order of 10^{-6} S/cm, at 0 °C is impressive.

Future work will attempt to further characterize the rotational and diffusional motions in the solid phases by NMR and also to investigate the conductive properties of dopant ions in these structures.

Appendix

Synthetic and Characterization Details. *1,1-Dimethyl Pyrrolidinium Iodide (P_{11}−I).* An amount of 6.30 g (0.069 mol) 1-methyl pyrrolidine (Aldrich, all chemicals were used as received except as otherwise specified) was mixed with 15 g acetonitrile (Fluka); 12.08 g (0.085 mol) iodomethane (Aldrich) was added dropwise into the pyrrolidine solution, and N_2 bubbling was used. The mixture was stirred at room temperature overnight. The solvent was removed by distillation, and the solid product was washed with petroleum spirit X4 three times. The final product was dried under vacuum at room temperature for more than 48 h, and 14.9 g of the product was obtained (yield 95%). ^{1}H NMR (D_2O, δ/ppm relative to TMS): 3.57−3.52 (m, 4H), 3.17 (s, 6H), 2.26−2.24 (m, 4H).

1-Ethyl-1-methyl Pyrrolidinium Iodide (P_{12}−I). The same procedure was used as in P_{11}−I. 1-Iodoethane (Aldrich) was used instead of iodomethane (yield 65%). ^{1}H NMR (D_2O, δ/ppm relative to TMS): 3.54−3.41 (m, 6H), 3.05 (s, 6H), 2.23−2.22 (m, 4H), 1.42−1.36 (m, 3H).

1-Methyl-1-n-propyl Pyrrolidinium Iodide (P_{13}−I). The same procedure was used as in P_{11}−I. 1-Iodopropane (Aldrich) was used instead of iodomethane, and the reacting mixture was stirred at ∼60 °C (oil bath) instead of room temperature (yield 86%). ^{1}H NMR (D_2O, δ/ppm relative to TMS): 3.54−3.52 (m, 4H), 3.34−3.28 (m, 2H), 3.05 (s, 6H), 2.30−2.14 (m, 4H), 1.89−1.76 (m, 2H), 0.98 (t, 3H, J = 7.4 Hz).

1-n-Butyl-1-methyl Pyrrolidinium Iodide (P_{14}−I). The same procedure was used as in P_{11}−I. 1-Iodobutane (Aldrich) was used instead of iodomethane, and the reacting mixture was stirred at ∼70 °C (oil bath) instead of room temperature (yield 96%). ^{1}H NMR (D_2O, δ/ppm relative to TMS): 3.54−3.51 (m, 4H), 3.38−3.33 (m, 2H), 3.05 (s, 6H), 2.28−2.15 (m, 4H), 1.84−1.73 (m, 2H), 1.41 (sextuplet, 2H, J = 7.4 Hz), 0.95 (t, 3H, J = 7.4 Hz).

1,1-Dimethyl Pyrrolidinium Bis(trifluoromethane Sulfonyl) Imide Salt (P_{11}). An amount of 1.60 g (0.0056 mol) lithium bis(trifluoromethane sulfonyl) imide salt (3 M) was dissolved in 2 g distilled water. In 2 g distilled water, 1.27 g (0.0056 mol) 1,1-dimethyl pyrrolidinium iodide was dissolved. The two aqueous solutions were mixed together and then stirred at room temperature for 3 h. The product (organic phase) was separated from the aqueous phase by a separating funnel and was washed with distilled water twice to remove any water-soluble impurities. The final product was dried under vacuum at room temperature, and 1.79 g of the product was obtained (yield 84%). ^{1}H NMR (DMSO-d_6, δ/ppm relative to TMS): 3.46−3.43 (m, 4H), 3.08 (s, 6H), 2.12−2.07 (m, 4H).

In all of the following, the same procedure as above for P_{11} was used, substituting the appropriate pyrrolidinium iodide starting material.

1-Ethyl-1-methyl Pyrrolidinium Bis(trifluoromethane Sulfonyl) Imide Salt (P_{12}). Yield 94%. ^{1}H NMR (DMSO-d_6, δ/ppm relative to TMS): 3.48−3.38 (m, 6H), 2.96 (s, 6H), 2.11−2.07 (m, 4H), 1.29−1.24 (m, 3H).

1-Methyl-1-n-propyl Pyrrolidinium Bis(trifluoromethane Sulfonyl) Imide Salt (P_{13}). Yield 86%. Anal. Calcd for $C_{10}H_{18}N_2F_6S_2O_4$: C, 29.41; H, 4.44; N, 6.86; F, 27.92; S, 15.70; O, 15.67. Found: C, 29.47; H, 4.69; N, 6.93; F, 27.98; S, 15.85; O, 15.08. ^{1}H NMR (DMSO-d_6, δ/ppm relative to TMS): 3.51−3.39 (m, 4H), 3.28−3.24 (m, 2H), 2.99 (s, 3H), 2.10−2.08 (m, 4H), 1.78−1.68 (m, 2H), 0.92 (t, 3H, J = 7.4 Hz).

1-n-Butyl-1-methyl Pyrrolidinium Bis(trifluoromethane Sulfonyl) Imide Salt (P_{14}). Yield 88%. ^{1}H NMR (DMSO-d_6, δ/ppm relative to TMS): 3.52−3.39 (m, 4H), 3.33−3.27 (m, 2H), 2.98 (s, 6H), 2.15−2.04 (m, 4H), 1.74−1.64 (m, 2H), 1.32 (sextuplet, 2H, J = 7.4 Hz), 0.94 (t, 3H, J = 7.4 Hz).

References and Notes

(1) Xu, K.; Zhang, S.; Angell, C. A. *J. Electrochem. Soc.* **1996**, *143* (11), 3548−3554.

(2) Liu, C.; Angell, C. A. *Solid State Ionics* **1996**, *86*−*88*, 467−473.

(3) Xu, K.; Day, N. D.; Angell, C. A. *J. Electrochem. Soc.* **1996**, *143* (9), L209−L211.

(4) Angell, C. A.; Xu, K.; Liu, C. Arizona State University; U.S. Patent 548,670 A.

(5) Bonhote, P.; Dias, A. P.; Papageorgiou, N.; Kalyanasundaram, K.; Gratzel, M. *Inorg. Chem.* **1996**, *35*, 1168.

(6) (a) Wilkes, J. S.; Levisky, J. A.; Wilson, R. A.; Hussey, Ch. L. *Inorg. Chem.* **1982**, *21*, 1263. (b) Wilkes, J. S.; Zaworotko, M. J. *J. Chem. Soc. Chem. Commun.* **1992**, 965.

(7) Matsunaga, M.; Inoue, Y.; Morimitsu, M.; Hosokawa, K. *Proc. Electrochem. Soc.* **1993**, *93*−*99* (Molten Salt Chemistry and Technology), 507.

(8) Seddon, K. R. *J. Chem. Technol. Biotechnol.* **1997**, *68*, 351−356.

(9) Fuller, J.; Carlin, R. T.; De Long, H. C.; Haworth, D. *J. Chem. Soc., Chem. Commun.* **1994**, 299.

(10) Sun, J.; Forsyth, M.; MacFarlane, D. R. *Ionics* **1997**, *3*, 356.

(11) Sun, J.; Forsyth, M.; MacFarlane, D. R. *J. Phys. Chem.* **1998**, *102*, 8858.

(12) Sun, J.; Forsyth M.; MacFarlane, D. R. *Molten Salt Forum* **1998**, *5*−*6*, 585−588.

(13) MacFarlane, D. R.; Sun, J.; Forsyth, M.; Meakin, P.; Amini, N. In preparation.

(14) Golding, J.; MacFarlane, D. R.; Spiccia, L.; Forsyth, M.; Skelton, B. W.; White, A. H. *Chem. Commun.* **1998**, *15*, 1593−1594.

(15) Elias, A. M.; Elias, M. E. *Molten Salt Forum* **1998**, *5*−*6*, 617.

(16) Angell, C. A. *Annu. Rev. Phys. Chem.* **1992**, *43*, 693.
(17) Hattori, M.; Fukada, S.; Nakamura, D.; Ikeda, R. *J. Chem. Soc., Faraday Trans.* **1990**, *86*, 3777.
(18) Iwai, S.; Hattori, M.; Nakamura, D.; Ikeda, R. *J. Chem. Soc., Faraday Trans.* **1993**, *89*, 827.
(19) Ishida, H.; Furukawa, Y.; Kashino, S.; Sato, S.; Ikeda, R. *Ber. Bunsen-Ges. Phys. Chem.* **1996**, *100*, 433−439.
(20) Tanabe, T.; Nakamura, D.; Ikeda, R. *J. Chem. Soc., Faraday Trans.* **1991**, *87* (7), 987−990.
(21) Shimizu, T.; Tanaka, S.; Onoda-Yamamuro, N.; Ishimaru, S.; Ikeda, R. *J. Chem. Soc., Faraday Trans.* **1997**, *93* (2), 321−326.
(22) Cooper, E. I.; Angell, C. A. *Solid State Ionics* **1986**, *18/19*, 570.
(23) Timmermans, J. *J. Phys. Chem. Solids*, **1961**, *18*, 1.
(24) Atake, T.; Angell, C. A. *J. Phys. Chem.* **1979**, *83* (25), 3218−3223.
(25) Angell, C. A.; Busse, L. E.; Cooper, E. I.; Kadiyala, R. K.; Dworkin, A.; Ghelfenstein, M.; Szwarc, H.; Vassal, A. *J. Chem. Phys*. **1985**, *82*, 267−274.
(26) Angell, C. A. *J. Non-Cryst. Solids* **1991**, *131*−*133*, 13−31.
(27) Angell, C. A. *Pure Appl. Chem.* **1991**, *63* (10), 1387−1392.
(28) Fan, J.; Cooper, E. I.; Angell, C. A. *J. Phys. Chem.* **1994**, *98*, 9345−9349.